Nanorods of manganese oxides: Synthesis, characterization and catalytic application

ARTICLE *in* JOURNAL OF SOLID STATE CHEMISTRY · MARCH 2006

Impact Factor: 2.13 · DOI: 10.1016/j.jssc.2005.11.028

Available online at www.sciencedirect.com
SCIENCE DIRECT®
Journal of Solid State Chemistry 179 (2006) 679–684
JOURNAL OF SOLID STATE CHEMISTRY
www.elsevier.com/locate/jssc

Nanorods of manganese oxides: Synthesis, characterization and catalytic application

Zeheng Yang[a], Yuancheng Zhang[a], Weixin Zhang[a,*], Xue Wang[a], Yitai Qian[a], Xiaogang Wen[b], Shihe Yang[b,*]

[a]*School of Chemical Engineering, Hefei University of Technology, Hefei, Anhui 230009, PR China*
[b]*Department of Chemistry and Institute of Nano Science and Technology, The Hong Kong University of Science and Technology, Clear Water Bay, Kowloon, Hong Kong, PR China*

Received 30 August 2005; received in revised form 13 November 2005; accepted 18 November 2005
Available online 18 January 2006

Abstract

Single-crystalline nanorods of β-MnO_2, α-Mn_2O_3 and Mn_3O_4 were successfully synthesized via the heat-treatment of γ-MnOOH nanorods, which were prepared through a hydrothermal method in advance. The calcination process of γ-MnOOH nanorods was studied with the help of Thermogravimetric analysis and X-ray powder diffraction. When the calcinations were conducted in air from 250 to 1050 °C, the precursor γ-MnOOH was first changed to β-MnO_2, then to α-Mn_2O_3 and finally to Mn_3O_4. When calcined in N_2 atmosphere, γ-MnOOH was directly converted into Mn_3O_4 at as low as 500 °C. Transmission electron microscopy (TEM) and high-resolution TEM were also used to characterize the products. The obtained manganese oxides maintain the one-dimensional morphology similar to the precursor γ-MnOOH nanorods. Further experiments show that the as-prepared manganese oxide nanorods have catalytic effect on the oxidation and decomposition of the methylene blue (MB) dye with H_2O_2.

Keywords: Manganese oxides; Nanorods; Catalysis

1. Introduction

Manganese oxides with a rather complex oxide system, forming several phases such as MnO, MnO_2, Mn_2O_3 and Mn_3O_4, are of considerable importance in many technological applications. Mn_2O_3 is known to be an active catalyst for removing carbon monoxide and nitrogen oxide from waste gas [1,2], MnO_2 and Mn_3O_4 for the oxidation of methane and carbon monoxide or the selective reduction of nitrobenzene [3–5]. Mn_2O_3 and Mn_3O_4 have also been used to produce soft magnetic materials, such as manganese zinc ferrite [6,7]. And in the last decade, considerable attention has been focused on lithiation of Mn-oxides for intercalation compounds of Li–Mn–O as electrode materials for rechargeable lithium batteries [8–12].

Recently, the synthesis of one-dimensional (1D) nanostructures has attracted considerable attention because 1D nanostructures have potential applications in wide-ranging sectors including catalysis, sensing, electronics and photoelectronics, with performances that are anticipated to be superior to those of their bulk counterparts [13,14]. For example, 1D nanostructured MnO_2 may provide the possibility of detecting the theoretical operating limits of a lithium battery as the 1D systems are the smallest dimension structures for efficient transport of electrons [15,16], and may give an ideal host material for the insertion and extraction of lithium ions. Suib et al. found that the catalytic performance of nanoribbon-like Mg-todorokite materials in converting benzyl alcohol to benzaldehyde was improved greatly compared to that of the bulk Mg-todorokite [17].

Many efforts are being made to prepare 1D nanostructured crystalline manganese oxides and several groups have reported the synthesis of 1D nanostructured manganese

*Corresponding authors. Fax: +86 551 2901450.
E-mail addresses: wxzhang@hfut.edu.cn (W. Zhang), chsyang@ust.hk (S. Yang).

0022-4596/$ - see front matter © 2005 Elsevier Inc. All rights reserved.
doi:10.1016/j.jssc.2005.11.028

oxides. Xie Yi et al. have obtained γ-MnO_2 nanowires by a hydrothermal chemical reaction of a coordination polymer $[\{Mn(SO_4)(4,4/\text{-bpy})(H_2O)_2\}_n]$ in NaOH solution [18]. Li Yadong has reported a hydrothermal method to synthesize single-crystalline α-MnO_2 nanowires and β-MnO_2 nanorods [19]. Yuan Zhongyuan et al. have synthesized single-crystalline α-Mn_2O_3 nanorods by ammonia-hydrothermal treatment of commercial granular/bulky MnO_2 [20]. Shao Changlu et al. used an electrospinning technique to get α-Mn_2O_3 and Mn_3O_4 nanofibers, which involves several steps such as preparation of a gel, electrospinning and calcination [21]. Wang Wenzhong et al. have synthesized Mn_3O_4 nanowires at 850 °C in NaCl flux through heat treatment of nanosized $MnCO_3$ precursors [22]. In last 2 years, several groups have reported the preparation of β-MnO_2 nanorods/nanowires and/or Mn_3O_4 nanorods/nanoparticles through a γ-MnOOH precursor route [23–27]. However, few systematic preparations of 1D nanostructured manganese oxides were reported.

In this paper, we report a systematic synthesis of manganese oxide nanorods via the heat-treatment of γ-MnOOH nanorod precursors, which were prepared through a hydrothermal method in advance. β-MnO_2, α-Mn_2O_3 and Mn_3O_4 nanorods with morphology similar to the precursors' are successfully obtained, respectively, through the heat-treatment of γ-MnOOH nanorods at different temperatures in air. Another important aspect of this work is the successful preparation of the Mn_3O_4 nanorods via the heat-treatment of γ-MnOOH nanorods under flowing N_2 atmosphere at much lower temperatures than in air. This innovation not only saves much energy but also is helpful for Mn_3O_4 sample to retain the nanorod morphology similar to the precursors'. Our approach requires neither complex apparatus nor sophisticated techniques. The successful synthesis of the γ-MnOOH nanorod precursor in a large-sized autoclave (1 L) via hydrothermal reactions has provided the advantage for the large-scale preparation of 1D nanostructured manganese oxides, which is essential for application study. Further experiments reveal that the as-prepared manganese oxide nanorods show catalytic efficiency in the oxidation and decomposition of the methylene blue (MB) dye with H_2O_2.

2. Experimental section

2.1. Preparation of nanostructured precursor γ-MnOOH

The reagents $KMnO_4$ and CH_3CH_2OH are analytical grade from Shanghai Chemicals Company and were used without further purification. The preparation of the precursor γ-MnOOH nanorods was similar to our previous report [28]. In a typical procedure, 4 g of $KMnO_4$, 4 mL of CH_3CH_2OH and 400 mL of distilled water were put in a stainless steel autoclave of 1 L capacity with a magnetic stirrer and then the autoclave was sealed and kept at 100–150 °C for 24 h with a stirring rate of about 200 r/min, then it was allowed to cool to room temperature naturally. The product was collected after washing, filtering and drying in vacuum.

2.2. Preparation of manganese oxides

The as-prepared γ-MnOOH precursor was subsequently calcined in the temperature range of 250–1050 °C in a furnace for 4–16 h to get manganese oxides: β-MnO_2, α-Mn_2O_3 and Mn_3O_4 (see Table 1). In parallel, Mn_3O_4 was also prepared through calcining γ-MnOOH precursor under flowing N_2 atmosphere at 500–800 °C for 4–16 h.

2.3. Physical analysis

Thermogravimetric analysis (TGA) was carried on a Shimadzu TGA-50H thermogravimeter analyzer to determine the thermal behavior of the γ-MnOOH precursors. The experiments were conducted under an air atmosphere (20 mL/min) at a heating rate of 10 °C/min. X-ray powder diffraction (XRD) patterns were recorded on a Japan Rigaku D/max-γB X-ray diffractometer with Cu Kα radiation ($\lambda = 1.54178$ Å), operated at 40 kV and 80 mA. Transmission electron microscopy (TEM) images and electron diffraction (ED) images were taken with a Hitachi H-800 transmission electron microscope, performed at an accelerating voltage of 200 kV. The high-resolution TEM (HRTEM) observation was performed with a 200 kV electron microscope on JEOL-2010.

Table 1
Reaction conditions and corresponding products

Reaction temperature (°C)	Reaction time (h)	Reaction atmosphere	Composition of the products (XRD result)
250	3	Air	β-MnO_2 + MnOOH
250–400	4–16	Air	β-MnO_2
550	4–8	Air	β-MnO_2 (main) + α-Mn_2O_3 (minor)
550	8–16	Air	α-Mn_2O_3 (main) + β-MnO_2 (minor)
600–800	8–16	Air	α-Mn_2O_3
850–950	8–16	Air	α-Mn_2O_3 + Mn_3O_4
1000–1050	8–16	Air	Mn_3O_4
400	4–8	N_2	MnOOH (main) + Mn_3O_4 (minor)
400	8–16	N_2	Mn_3O_4 (main) + MnOOH (minor)
500–800	4–16	N_2	Mn_3O_4

2.4. Catalytic measurements

The obtained manganese oxides were used as catalysts for the oxidation and decoloration of the MB dye with H_2O_2. The catalysts to be tested were dried at 110 °C overnight beforehand to remove moisture. The MB and H_2O_2 are of analytical purity from Shanghai Chemicals Company and were used as received without further purification. The catalytic reaction was carried out in a 500 mL glass flask, which contained 62.5 mL of MB dye solution (125 mg/L), 162.5 mL of distilled water, and 125 mg of manganese oxides catalysts. After adding 25 mL of 30% (weight percent) H_2O_2 solution, the flask was sealed and the mixture was allowed to react at room temperature with continuous magnetic stirring. For a given time interval, 1 mL of the mixture solution was pipetted into a volumetric flask and quickly diluted with distilled water to 25 mL prior to analysis. For optical absorption measurements, the diluted solution was immediately centrifuged in order to remove the catalyst particles, which tend to scatter the incident beam. The centrifuged solution was then put into a quartz cell (path length 1.0 cm) and the absorption spectrum was measured with a Shimadzu UV-2550 ultraviolet-visible (UV-Vis) spectrophotometer. A linear calibration curve for the dye concentrations was obtained by monitoring the peak intensity at $\lambda_{max} = 664$ nm for a series of standard solutions according to the Beer's law.

3. Results and discussion

First of all, TGA was carried out to investigate the thermal behavior of the γ-MnOOH nanorods in air so as to guide the calcination procedure for the preparation of the target products. As can be seen in Fig. 1, three distinct peaks appear at 282.9, 558.2 and 891.8 °C in the DTGA curve, which is the first derivative of the TGA curve with three corresponding weight-loss steps. The first weight loss starts at about 200 °C, showing a weight loss of 1.737%.

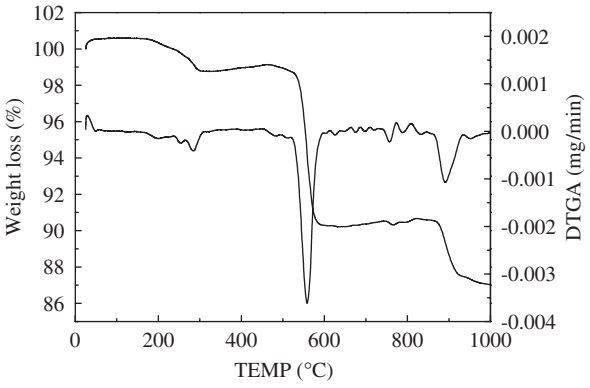

Fig. 1. Thermogravimetric analysis curves of the γ-MnOOH precursor in air.

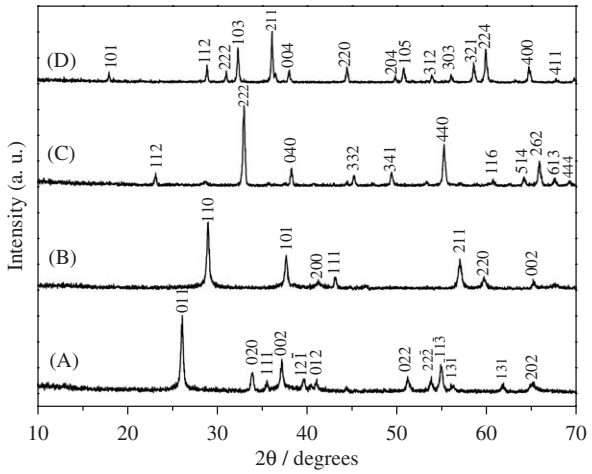

Fig. 2. The XRD patterns of the samples: (A) the precursor γ-MnOOH nanorods; (B) the sample obtained through calcining the γ-MnOOH precursor at 350 °C for 4 h in air; (C) the sample obtained through calcining the γ-MnOOH precursor at 600 °C for 12 h in air; (D) the sample obtained through calcining the γ-MnOOH precursor at 600 °C for 8 h in the N_2 flux.

The second weight change starts at about 460 °C with a weight loss of 8.839%. The third weight change starts at about 850 °C with a weight loss of 3.538%. XRD analysis and weight-loss calculations show that the three steps of weight change are associated with the conversion of γ-MnOOH to β-MnO_2, then to α-Mn_2O_3 and finally to Mn_3O_4, respectively.

Based on the TGA analysis, the calcination process of γ-MnOOH nanorods was further studied with the help of XRD. The results are listed in Table 1. When the calcinations were conducted in air from 250 to 1050 °C, the precursor γ-MnOOH changed from γ-MnOOH to β-MnO_2, β-MnO_2 to α-Mn_2O_3 and α-Mn_2O_3 to Mn_3O_4, and pure phases of β-MnO_2, α-Mn_2O_3 and Mn_3O_4 were obtained, respectively, at 250, 600 and 1000 °C. Moreover, when the calcination of γ-MnOOH nanorods was conducted under the flow of N_2 atmosphere, γ-MnOOH was directly converted into Mn_3O_4 at 500 °C, which is much lower than that for preparing Mn_3O_4 in air.

Fig. 2 gives the XRD patterns of the as-prepared products as well as the precursor γ-MnOOH nanorods. Fig. 2A exhibits the XRD pattern of the precursor γ-MnOOH nanorods. Fig. 2B and C show the XRD patterns of the products prepared through heating γ-MnOOH nanorods in air at 350 °C for 4 h and at 600 °C for 12 h, respectively. The diffraction peaks in patterns B and C can be indexed to pure tetragonal β-MnO_2 and pure orthorhombic phase of α-Mn_2O_3, respectively. Fig. 2D is the XRD pattern of the product resulted from heating γ-MnOOH in N_2 flux at 600 °C for 8 h. All diffraction peaks can be indexed to pure tetragonal Mn_3O_4. The corresponding lattice constants of the as-prepared products are shown in Table 2.

Table 2
Lattice constants of the as-prepared manganese oxides

Manganese oxides	Crystal system	Calculated value			Theoretical value			
		a (Å)	*b* (Å)	*c* (Å)	*a* (Å)	*b* (Å)	*c* (Å)	JCPDS card
β-MnO_2	Tetragonal	4.4010		2.8700	4.3999		2.8740	No. 24-0735
α-Mn_2O_3	Orthorhombic	9.4080	9.4119	9.4066	9.4161	9.4237	9.4051	No. 24-0508
Mn_3O_4	Tetragonal	5.7680		9.4720	5.7621		9.4696	No. 24-0734

According to our experimental results, the following chemical equations may help to describe the preparation mechanism.

(1) Oxidation of γ-MnOOH to β-MnO_2 in air at 250–550 °C

$$4\gamma\text{-MnOOH(s)} + O_2(g) \rightarrow 4\beta\text{-}MnO_2(s) + 2H_2O(g). \quad (1)$$

(2) Decomposition of β-MnO_2 into α-Mn_2O_3 at 550–900 °C

$$4\beta\text{-}MnO_2(s) \rightarrow 2\alpha\text{-}Mn_2O_3(s) + O_2(g). \quad (2)$$

(3) Further decomposition of α-Mn_2O_3 into Mn_3O_4 at above 900 °C

$$3\alpha\text{-}Mn_2O_3(s) \rightarrow 2Mn_3O_4\ (s) + 1/2O_2(g). \quad (3)$$

The above manganese oxide phase changes and their transition temperatures are similar to those reported in the literature [29].

(4) Decomposition of γ-MnOOH into Mn_3O_4 in N_2 flux

$$12\gamma\text{-MnOOH(s)} \rightarrow 4Mn_3O_4(s) + O_2(g) + 6H_2O(g). \quad (4)$$

Different from the case in air, when calcined in N_2 flux, γ-MnOOH can be directly converted into Mn_3O_4 at 500 °C, as described in Eq. (4). Here N_2 flux not only prevents the oxidation of γ-MnOOH by O_2 from the air, but also takes away the O_2 generated from the decomposition reaction (Eq. (4)), and makes the reaction (Eq. (4)) go towards the right side easily. So, under this condition, γ-MnOOH can be directly converted into Mn_3O_4 at 500 °C. This innovation not only saves much energy but also is helpful for Mn_3O_4 sample to retain the nanorod morphology similar to the precursor's, since high-temperature calcination may change or destroy the morphology and structure of the products to some extent, which has been confirmed by TEM observation (see Supplementary materials).

Fig. 3 shows the TEM and HRTEM images of the prepared samples. Fig. 3A is the TEM image of the precursor γ-MnOOH nanorods, with diameters of 20–450 nm and lengths of tens of micrometers. Fig. 3B, C and D show the TEM images of β-MnO_2 prepared in air at 350 °C for 4 h, α-Mn_2O_3 prepared in air at 600 °C for 12 h, and Mn_3O_4 prepared in N_2 atmosphere at 600 °C for 8 h, respectively. The obtained manganese oxides maintain the 1D morphology similar to the precursor γ-MnOOH nanorods, with diameters of tens to hundreds of nanometers and lengths of tens of micrometers. Fig. 3E, F, G and H display the typical nanorod TEM images of γ-MnOOH, β-MnO_2, α-Mn_2O_3 and Mn_3O_4 samples, respectively. The single-crystalline nature of the obtained nanorods can be verified by the corresponding ED patterns (insets in Fig. 3E, F, G and H). The HRTEM images of each nanorod are also displayed correspondingly in the insets of Fig. 3E, F, G and H, showing that the resultant nanorods are structurally uniform. The ED patterns and the HRTEM images of these nanorods help us to get information of the growth. For γ-MnOOH, the interplanar distance of fringes perpendicular to the nanorod axis is 2.88 Å, corresponding to the (101) planes of monoclinic MnOOH. The MnOOH nanorods grow along the [101] crystal direction. For β-MnO_2, the interplanar distance of fringes perpendicular to the nanorod axis is 2.84 Å, corresponding to the (001) planes of tetragonal β-MnO_2, which stands for the growth direction [001]. For α-Mn_2O_3, the interplanar spacing of the fringes marked by arrows is 6.60 Å, corresponding to the $(\bar{1}10)$ planes of orthorhombic α-Mn_2O_3. The growth direction of the nanorod is along the [101]. For Mn_3O_4, the interplanar spacing of the fringes perpendicular to the rod axis is 3.10 Å, corresponding to the (112) planes of tetragonal Mn_3O_4, which stands for the growth direction [112].

The catalytic performances of the three kinds of manganese oxide nanorods have been studied on the oxidation and decomposition of MB dye with H_2O_2 under controlled conditions. By monitoring the MB absorption at the peak wavelength 664 nm, we obtained the decoloration degree of MB shown in Fig. 4. Here the degree of decoloration is expressed as $(I_0-I)/I_0$, where I_0 is the absorption at $t = 0$ and I is the absorption at a given reaction time. The three kinds of manganese oxide nanorods have catalytic effects on the oxidation and decomposition of MB with H_2O_2. After 150 min of reaction, the decoloration degree of MB dye for β-MnO_2, Mn_3O_4 and α-Mn_2O_3 nanorod catalysts are about 98%, 85% and 73%, respectively. To prove the catalysis effect, we have done the following comparison experiments (see Supplementary materials). In the absence of any catalysts (only MB + H_2O_2), no obvious dye decoloration is observed after 2 h. With the β-MnO_2 nanorods but no H_2O_2 (only MB + β-MnO_2 nanorods), the degree of decoloration

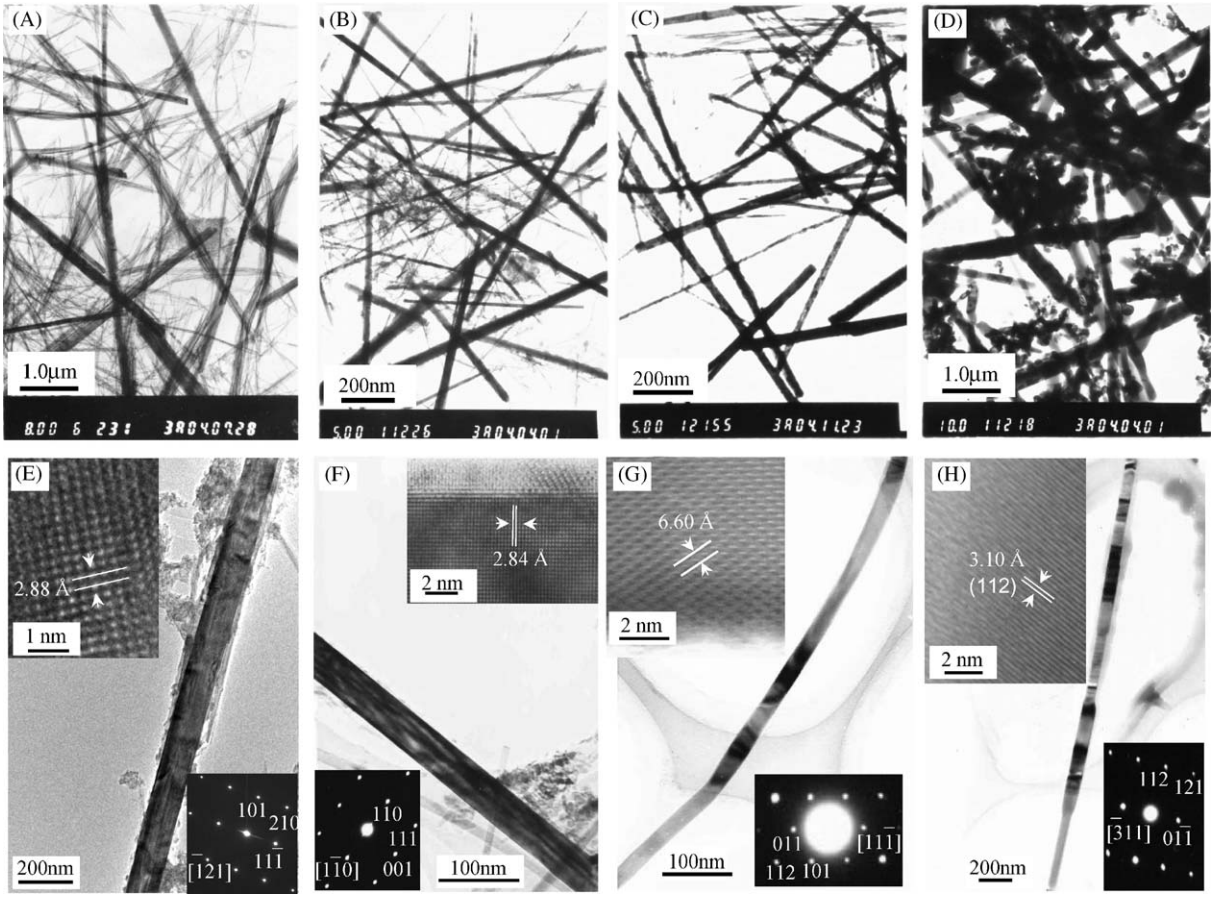

Fig. 3. TEM images of the as-prepared manganese oxides: (A) γ-MnOOH nanorods; (B) β-MnO_2 nanorods; (C) α-Mn_2O_3 nanorods; (D) Mn_3O_4 nanorods; (E) a single MnOOH nanorod, insets are the corresponding SAED pattern and HRTEM image; (F) a single β-MnO_2 nanorod, insets are the corresponding SAED pattern and HRTEM image; (G) a single α-Mn_2O_3 nanorod, insets are the corresponding SAED pattern and HRTEM image; (H) a single Mn_3O_4 nanorod, insets are the corresponding SAED pattern and HRTEM image.

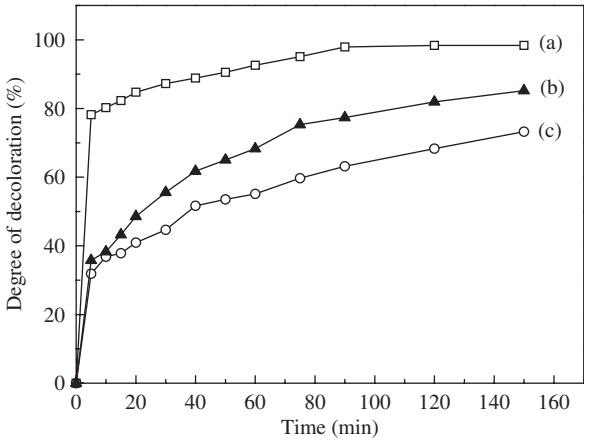

Fig. 4. Time profiles of MB decoloration. (a) MB + H_2O_2 + β-MnO_2 nanorods; (b) MB + H_2O_2 + Mn_3O_4 nanorods; (c) MB + H_2O_2 + α-Mn_2O_3 nanorods.

reaches about 30% within 15 min and then tends to be saturated, which can be ascribed to adsorption of the dye molecules on the β-MnO_2 nanorods. When both β-MnO_2 catalyst and H_2O_2 oxidant were added to the MB solution, obvious decoloration occurred. Remarkably, the use of β-MnO_2 nanorods as a catalyst increased the degree of decoloration to 82.3% in only 15 min. The saturated degree of decoloration was as high as 98.3%. Catalytic decoloration of MB must have occurred here, because simple adsorption on the surfaces of the nanorods can only account for ~30% of the decoloration. On the other hand, XRD analyses indicate that the manganese oxides have no structure changes before and after the catalytic reactions. The differences in their catalytic activities among the β-MnO_2, Mn_3O_4 and α-Mn_2O_3 nanorod catalysts may result from the difference of their surface areas and active sites. Further investigations on the mechanism of the manganese oxide catalytic reaction are ongoing.

4. Conclusion

In summary, a simple synthetic approach has been used to prepare manganese oxide nanorods. β-MnO_2, α-Mn_2O_3 and Mn_3O_4 nanorods have been obtained, respectively, through calcining γ-MnOOH nanorods in air or under flowing N_2 atmosphere. When the calcinations are conducted in air from 250 to 1050 °C, the precursor γ-MnOOH undergoes the changes from γ-MnOOH to β-MnO_2, then

to α-Mn_2O_3 and finally to Mn_3O_4. When the calcination of γ-MnOOH nanorods is conducted under the flow of N_2 atmosphere, γ-MnOOH can be directly converted into Mn_3O_4 at as low as 500 °C. The obtained manganese oxides maintain the 1D morphology similar to the precursor γ-MnOOH nanorods, with diameters of tens to hundreds of nanometers and lengths of tens of micrometers. The obtained manganese oxide nanorods show catalytic effects on the oxidation and decoloration of the MB dye with H_2O_2. This facile and systematic synthesis method is capable for large-scale preparation of 1D nanostructured manganese oxides and may probably extend to the synthesis of other transition metal oxides.

Acknowledgments

This work was supported by the National Natural Science Foundation of China (NSFC 20301005, 20576024), Anhui Provincial Natural Science Foundation (00045112) and the Excellent Young Teachers Program of the Ministry of Education of China.

Appendix A. Supplementary materials

Supplementary data associated with this article can be found in the on-line version at doi:10.1016/j.jssc.2005.11.028

References

[1] M. Baldi, Appl. Catal. B Environ. 17 (1998) L175.
[2] H.M. Zang, Y. Teraoka, Catal. Today 6 (1989) 155.
[3] L. Dimesso, L. Heider, H. Hahn, Solid State Ionics 123 (1999) 39.
[4] E.R. Stobhe, B.A.D. Boer, J.W. Geus, Catal. Today 47 (1999) 161.
[5] E. Grootendorst, Y. Verbeek, V. Ponce, J. Catal. 157 (1995) 706.
[6] V.V. Pankov, Ceram. Int. 14 (1988) 87.
[7] Y. Fujoimura, Jpn. Kokai Tokyo Koho JP 08, 310, 857, May 1995.
[8] M.M. Thackeray, W.I.F. David, P.G. Bruce, J.B. Goodenough, Mater. Res. Bull. 18 (1983) 461.
[9] S.T. Myung, S. Komaha, N. Kumagai, Electrochim. Acta 47 (2002) 3287.
[10] L. Sanchez, J.-P. Pereira-Ramos, Electrochim. Acta 42 (1997) 531.
[11] M. Tabuchi, K. Ado, J. Electrochem. Soc. 145 (1998) L49.
[12] T. Nakamura, A. Kajiyama, Solid State Ionics 45 (1999) 124.
[13] A.J. Zarur, J.Y. Ying, Nature 403 (2000) 65.
[14] S.F. Yin, B.Q. Xu, C.F. Ng, C.T. Au, Appl. Catal. B: Environ. 48 (2004) 237.
[15] J. Hu, T.W. Odom, C.M. Lieber, Acc. Chem. Res. 32 (1999) 435.
[16] M.H. Huang, S. Mao, H. Feick, H.Q. Yan, Y.Y. Wu, H. Kind, E. Weber, R. Russo, P.D. Yang, Science 292 (2001) 1897.
[17] J. Liu, J. Cai, Y.C. Son, Q. Gao, S.L. Suib, M. Aindow, J. Phys. Chem. B. 106 (2002) 9761.
[18] Y. Xiong, Y. Xie, Z. Li, C. Wu, Chem. Eur. J. 9 (2003) 1645.
[19] X. Wang, Y.D. Li, J. Am. Chem. Soc. 124 (2002) 2880.
[20] Z.Y. Yuan, T.Z. Ren, G.H. Du, B.L. Su, Chem. Phys. Lett. 389 (2004) 83.
[21] C.L. Shao, H.Y. Guan, Y.C. Liu, X.L. Li, X.H. Yang, J. Solid State Chem. 177 (2004) 2628.
[22] W.Z. Wang, C.K. Xu, G.H. Wang, Y.K. Liu, C.L. Zheng, Adv. Mater. 14 (2002) 837.
[23] G.C. Xi, Y.Y. Peng, Y.C. Zhu, L.Q. Xu, W.Q. Zhang, W.C. Yu, Y.T. Qian, Mater. Res. Bull. 39 (2004) 1641.
[24] Y.C. Zhang, T. Qiao, X.Y. Hu, J. Solid State Chem. 177 (2004) 4093.
[25] Y.C. Zhang, T. Qiao, X.Y. Hu, W.D. Zhou, J. Cryst. Growth 280 (2005) 652.
[26] Y.G. Zhang, Y. Liu, F. Guo, Y.H. Hu, X.Z. Liu, Y.T. Qian, Solid State Commun. 134 (2005) 523.
[27] B. Folch, J. Larionova, Y. Guari, C. Guerin, C. Reibel, J. Solid State Chem. 178 (2005) 2368.
[28] W.X. Zhang, Z.H. Yang, Y. Liu, S.P. Tang, X.Z. Han, M. Chen, J. Cryst. Growth 263 (2004) 394.
[29] W.L. He, Y.C. Zhang, X.X. Zhang, H. Wang, H. Yan, J. Cryst Growth 252 (2003) 285.